Available online at www.sciencedirect.com
SCIENCE DIRECT®
Polymer 45 (2004) 3329–3340
polymer
www.elsevier.com/locate/polymer

Understanding polyanhydride blend phase behavior using scattering, microscopy, and molecular simulations

Matt J. Kipper[a], Soenke Seifert[b], P. Thiyagarajan[c], Balaji Narasimhan[a,*]

[a]*Department of Chemical Engineering, Iowa State University, 2035 Sweeney Hall, Ames, IA 50011-2230, USA*
[b]*Advanced Photon Source, Argonne National Laboratory, 9700 S. Cass Avenue, Argonne, IL 60439, USA*
[c]*Intense Pulsed Neutron Source, Argonne National Laboratory, 9700 S. Cass Avenue, Argonne, IL 60439, USA*

Received 17 October 2003; received in revised form 15 March 2004; accepted 17 March 2004

Abstract

The phase behavior of a biocompatible binary polyanhydride blend system composed of poly[1,6-bis(*p*-carboxyphenoxy)hexane] (poly(CPH)) and poly(sebacic acid) (poly(SA)) is described. The phase behavior is determined from the CPH-SA segmental interaction parameter, χ, obtained from in situ small angle X-ray scattering (SAXS) experiments. The predicted phase diagram has an upper critical solution temperature (UCST) with a critical point of 114 °C. The phase diagram is validated by optical microscopy (cloud point determination) of blend films. However, the full range of blend compositions is not accessible via cloud point measurements, because the melting point of poly(CPH) is above the critical point. Additionally, the poly(CPH) crystallinity interferes with cloud point determination because the length scale of the amorphous phase separation and that of the crystallinity are both near the limit of resolution of the optical microscope. The poly(CPH)-rich region of the phase diagram was investigated by ex situ atomic force microscopy on thin blend films. Finally, in order to validate the use of molecular simulations to study energetic and structural properties of this system, χ is also computed from molecular dynamics both above and below the critical point. Excellent agreement is obtained for all three experimental methods and the computational technique. The results are compared to a simple group contribution method for computing the solubility parameters of the polymers. This technique fails to accurately predict the phase diagram.

Keywords: Polyanhydrides; Polymer blend phase behavior; SAXS

1. Introduction

The use of multicomponent polymeric materials for drug delivery offers the potential to provide tailored drug release profiles [1–4], drug stabilization [5], and drug targeting [6]. However, multicomponent polymer systems often exhibit phase separation, and many of the properties of interest are governed by the phase behavior of the material. Though phase separation may be exploited to achieve desired characteristics in a particular system, if poorly understood, it may also have effects on the ability of a device to control the drug release profile [7,8]. Thus, design of drug delivery devices based on multicomponent polymer systems requires a detailed understanding of the phase behavior of the system of interest.

Biodegradable polymers have found widespread acceptance as carriers for therapeutic compounds. In particular, many researchers have focused on poly(ester)s such as poly(lactide-*co*-glycolide) and poly(ether)s such as poly(ethylene oxide) as biomaterials for drug delivery, due to their biocompatibility. These systems are hydrophilic and release encapsulated drugs via bulk erosion. We are interested in drug release from hydrophobic systems. Hydrophobic biodegradable systems exhibit surface-erosion, which may stabilize macromolecular drugs [9,10]. They also have release profiles governed by the erosion kinetics, rather than diffusion and swelling, as is the case for hydrophilic, bulk-eroding systems. Polyanhydrides are ideal because the chemistry of the monomer units can be made hydrophobic, while the polyanhydride bond in the backbone remains hydrolytically labile. Polyanhydrides have been shown to have good biocompatibility. (See the recent reviews by Katti et al. [11] and Narasimhan and Kipper [12].)

* Corresponding author. Tel.: +1-515-294-8019; fax: +1-515-294-2689.
E-mail address: nbalaji@iastate.edu (B. Narasimhan).

0032-3861/$ - see front matter © 2004 Published by Elsevier Ltd.
doi:10.1016/j.polymer.2004.03.052

We are interested in polyanhydrides composed of the monomers 1,6-bis(*p*-carboxyphenoxy)hexane (CPH) and sebacic acid (SA) (Fig. 1). These two materials erode at vastly different rates offering the opportunity to tailor release profiles by altering the composition [4,8,13].

We have previously characterized the crystallinity of poly(CPH:SA) copolymers [13,14], the effects of drug loading on crystallinity [13], and the drug release kinetics of both microspheres [4,15] and tablet [8] devices. Others have studied the release kinetics of similar polyanhydride systems, without providing details of the phase behavior [1,16]. Our previous work [8,17] has revealed that release from the individual phases determines drug release profiles from surface-erodible, two-component systems when the two phases have different release kinetics. In surface-erodible multicomponent systems, drug release may either lead or lag the overall polymer erosion rate. The drug release kinetics is only explained by considering the release kinetics from the individual phases. In phase-separated systems, the drug release kinetics is governed by the phase behavior of the polymer system, the relative erosion rates of the constituent phases, the partition coefficient of the drug in the two phases, and the composition (relative amounts of the two phases) [17]. Thus, a comprehensive description of the release mechanisms requires intimate knowledge of the phase behavior.

The miscibility of several polyanhydride systems has been qualitatively assessed experimentally by Domb [18], who investigated a variety of polyanhydride blends both in solution and melt. The miscibility of polyanhydrides with polyesters and polyethers has been studied by Shakesheff et al. [19], Chen et al. [20], and Chan and Chu [21]. However, the phase behavior of binary polyanhydride systems has not yet been comprehensively investigated. Our previous work has shown preliminary evidence that microphase separation exists in random copolymers of CPH and SA, and that this microphase separation affects the release profiles of dissolved drugs when the drugs partition in the two-phase system [8,17].

In the present study, we determine the phase diagram of the poly(CPH)/poly(SA) blend system. The phase diagram is predicted from the CPH-SA segmental interaction parameter, χ, determined from small-angle X-ray scattering (SAXS). The phase diagram is verified by optical microscopy and atomic force microscopy (AFM). The experimental work is complemented by the prediction of the poly(CPH)/poly(SA) blend phase behavior from molecular dynamics. Molecular dynamics also allows the prediction of the interaction parameter in the phase-separated region, which SAXS cannot do. This prediction is compared to the SAXS data, in order to validate the molecular dynamics technique. Knowledge of the phase behavior of the blend system will be extended to copolymer systems (both random and block) in future work as we design new polyanhydride copolymers with precisely tailored architectures for drug delivery.

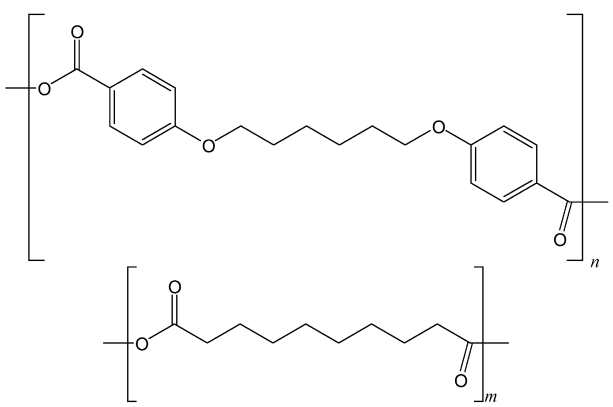

Fig. 1. Chemical structures of poly(CPH) (top) and poly(SA) (bottom).

2. Theoretical background

2.1. Polymer miscibility

The Flory–Huggins theory for predicting the miscibility of polymers A and B calculates the Gibbs' free energy of mixing, ΔG_{mix}, as [22]

$$\frac{\Delta G_{\mathrm{mix}}}{RT} = \frac{\phi_{\mathrm{A}}}{N_{\mathrm{A}}} \ln \phi_{\mathrm{A}} + \frac{\phi_{\mathrm{B}}}{N_{\mathrm{B}}} \ln \phi_{\mathrm{B}} + \chi_{\mathrm{FH}} \phi_{\mathrm{A}} \phi_{\mathrm{B}} \tag{1}$$

In Eq. (1) the ϕ's are the volume fractions of polymer A and B and the N's are their degrees of polymerization. The Flory–Huggins interaction parameter, χ_{FH}, represents the enthalpic component of the free energy of mixing. Note that volume change on mixing is neglected and the entropic terms only include combinatorial entropy. Because the entropic components are small and always favor mixing, χ_{FH} is a very important parameter.

In the original Flory–Huggins theory, χ_{FH} is predicted by [22]

$$\chi_{\mathrm{FH}} = Z V_{\mathrm{seg}} \frac{\Delta \tilde{E}_{\mathrm{mix}}}{RT} \tag{2}$$

In Eq. (2), $\Delta \tilde{E}_{mix}$ is the energy of mixing per pair of monomers, scaled by the unit volume, Z represents the lattice coordination number and V_{seg} is the volume of a mole of lattice sites. For off-lattice fluids, the coordination number loses some physical significance and becomes an adjustable parameter [23]. Methods to predict Z have been based on Monte Carlo packing algorithms that assume Z as the number of nearest-neighbor segments for each segment [24,25]. Use of Eq. (2) requires a prediction of the energy of mixing and assumes that the interaction parameter scales with reciprocal temperature.

Alternative temperature functionality can be introduced by modifying the equation for χ_{FH} resulting in a generalized

interaction parameter, χ, such as

$$\chi = A + \frac{B}{T} \tag{3}$$

A and B are empirical constants for a particular system but can be related to non-combinatorial entropic effects (A) and enthalpic interactions (B). Computational techniques for predicting χ rely on predictions of the energy of mixing.

The solubility parameter approach predicts miscibility based on the relative values of the Hildebrand solubility parameter, δ [26]. The solubility parameter is the square root of the cohesive energy density

$$\delta = \left(\frac{E_{coh}}{V}\right)^{1/2} \tag{4}$$

E_{coh} is the cohesive energy, which is defined as the increase in the potential energy of a system when all intermolecular interactions are turned off. δ can either be obtained experimentally or it can be predicted. Predictions usually rely on group contribution techniques (such as those reviewed in [27]) and experimental techniques involve comparing the solubility of the polymer of interest in solvents with known solubility parameters. The former technique may require a database of known compounds and does not account for the particular interactions between specific moieties in the materials of interest. The latter follows the line of reasoning that if A dissolves B and A dissolves C then B dissolves C. An alternative computational technique for obtaining E_{coh} is described below in the section on the Amorphous Cell algorithm.

Hildebrand and Scott [26] predict χ_{FH} as

$$\chi_{FH} = V_{seg}\frac{(\delta_A - \delta_B)^2}{RT} \tag{5}$$

The solubility parameter method can be used as a fast and simple screening method, but may provide misleading results when specific interactions between moieties in the two polymers (such as hydrogen bonds) that are not present in either of the homopolymers affect the solubility [28]. Another limitation is that since the interaction parameter computed from Eq. (5) is always positive, decreasing with temperature, and independent of composition, only UCST behavior can be predicted by this technique.

2.2. Small-angle X-ray scattering (SAXS)

SAXS experiments designed to probe the microstructure of amorphous polymers can be used to determine the interaction parameter. The intensity of scattered radiation, I, as a function of the scattering vector, $q(q = 4\pi \sin(\theta/2)/\lambda$; $\theta =$ scattering angle and λ is the wavelength of the incident radiation), is related to the structure factor, $S(q)$, which represents the root-mean-square electron concentration fluctuation by

$$\frac{1}{S(q)} = (\Delta\eta)^2\sigma_e V\frac{1}{I(q)} \tag{6}$$

Here $\Delta\eta$ is the difference in electron density between the two components, V is the volume of a monomer (chosen as an SA monomer in our study), and σ_e is the scattering cross section of an electron (6.653×10^{-9} Å^2). The electron densities are computed from the known mass densities of the polymers. (For the poly(CPH)/poly(SA) pair, $\Delta\eta =$ 0.0315, 0.0322, 0.0331 and 0.0341 e$^-$ Å^{-3} at 140, 150, 160, and 170 °C, respectively.) The structure factor is then related to the interaction parameter by de Gennes' random phase approximation [29].

$$S(q)^{-1} = \chi_s f_D^{-1}(q^2, R_\phi^2) - 2\chi \tag{7}$$

Here f_D is the Debye structure factor and R_ϕ^2 is the mean square radius of gyration. χ_s is the value of the interaction parameter at spinodal conditions. The parameters can be computed as [30,31]

$$\lim_{q\to 0}(f_D(q^2, R_\phi^2)) \approx N\left(1 - \frac{1}{3}q^2R_\phi^2\right) \tag{8}$$

$$R_\phi^2 = (1-\phi)R_A^2 + \phi R_B^2 \tag{9}$$

$$\chi_s = 0.5\left(\frac{1}{\sqrt{N_A}} + \frac{1}{\sqrt{N_B}}\right)^2 \tag{10}$$

Here N_A is the degree of polymerization of component A based on the monomer volume, V, in Eq. (6). (Because the volume of a CPH monomer is about twice that of the SA monomer, the monomer volume is taken as the volume of an SA monomer. Since the CPH monomer unit is symmetric, the degree of polymerization is computed assuming that monomer is half the CPH monomer shown in Fig. 1—essentially resulting in a head-to-head polymer). In Eq. (9), ϕ is the volume fraction of component A, and R_A^2 is the mean square radius of gyration of molecules in component A. Substituting Eq. (8) into Eq. (7), one obtains (for $\phi = 0.5$)

$$\lim_{q\to 0} S(q)^{-1} = 2[\chi_s - \chi(T)] + \frac{2\chi_s R_\phi^2}{3}q^2 \tag{11}$$

Linear extrapolation of the Zimm plot ($S^{-1}(q \to 0)$ vs. q^2) gives the interaction parameter (from the intercept) and the radius of gyration (from the slope in a q region where $qR_\phi < 1.3$). The approximation in Eq. (8) is valid in Guinier range ($I(q) \sim \exp(-Cq^2)$) that can be identified by a linear region in a Guinier plot (Ln[$I(q)$] vs. q^2) where $qR_\phi < 1.3$ [32].

2.3. Molecular dynamics (MD)

Case and Honeycutt review several computational techniques for studying the phase behavior of polymer systems [23]. Here we use the Amorphous Cell algorithm

available in the software package Materials Studio® from Accelrys Inc., which employs MD calculations, to predict the phase diagram of the poly(CPH)/poly(SA) blend system. This algorithm has been shown to be reliable for predicting bulk properties of polymeric systems [23,33–35]. We compare the MD predictions to a simple solubility parameter prediction technique. Our overall goal is to lay the foundation for studies aimed at characterizing blends of CPH-SA copolymers and drug solubilities and release kinetics from this polymer system.

The Amorphous Cell algorithm computes cohesive energy densities from MD simulations on models of bulk amorphous polymer systems [36]. Periodic boundary conditions are used to eliminate edge effects. As with any molecular simulation, it is imperative to begin with a reasonable starting configuration, since the CPU time required to simulate even very small times (e.g., nanoseconds) becomes prohibitively large for polymers [23]. Simulations are typically conducted over times on the order of picoseconds to a few nanoseconds on structures that are already assumed to be near equilibrium. Thus, the phenomena of mixing and de-mixing cannot be directly observed [36]. Rather, the energies of mixed and de-mixed configurations are compared to discern which is the more favorable. Theodorou and Suter [36] described an algorithm for the construction of amorphous cells based on a modified form of Flory's rotational isomeric states (RIS) theory [37]. Since then, some of their assumptions have been relaxed and the present model is fully atomistic, with no 'united-atom' groups. Bond stretching, angle bending, and out-of-plane bending are all allowed in addition to dihedral angle rotation. The temperature in the current model is explicit, rather than simply being implied by the density. And, the newer condensed-phase optimized molecular potentials for atomistic simulation studies (COMPASS) force field [38] is used, rather than the consistent valence force field (CVFF). The amorphous cells are equilibrated and evolved using molecular dynamics. The energy of mixing per unit volume is computed from the cohesive energy densities of the two homopolymers and the blend via

$$\Delta\tilde{E}_{\mathrm{mix}} = \phi_{\mathrm{A}}\left(\frac{E_{\mathrm{coh}}}{V}\right)_{\mathrm{A}} + (1-\phi_{\mathrm{A}}) \times \left(\frac{E_{\mathrm{coh}}}{V}\right)_{\mathrm{B}} - \left(\frac{E_{\mathrm{coh}}}{V}\right)_{\mathrm{blend}} \quad (12)$$

χ can then be computed from

$$\chi_{\mathrm{FH}} = V_{\mathrm{seg}}\frac{\Delta\tilde{E}_{\mathrm{mix}}}{RT} \quad (13)$$

The coordination number Z has been dropped (c.f. Eq. (2)) because in this algorithm $\Delta\tilde{E}_{\mathrm{mix}}$ is a bulk (rather than pairwise) energy of mixing per unit volume.

The advantage of this technique is that direct simulation of the bulk state can be obtained, with careful system construction. Therefore, any non-combinatorial entropic effects can be implicitly included in the enthalpic calculation. For example, if one is interested in volume changes on mixing, MD can be performed in the NPT ensemble, allowing the density to change. Additionally, enthalpic effects that may be unique to the blend system (i.e., interactions between pairs of atoms or groups that do not occur in the homopolymer systems) are accounted for. These are neglected in the solubility parameter approach.

3. Experimental

3.1. Materials

Sebacic acid (99%), *N*-methyl-2-pyrolidinone, and *p*-carboxy benzoic acid (99 + %) were purchased from Aldrich (Milwaukee, WI). 1,6-dibromohexane (98%) was purchased from Acros (Fairlawn, NJ). Acetic anhydride, chloroform, and methylene chloride were purchased from Fisher (Fairlawn, NJ) and deuterated chloroform was purchased from Cambridge Isotope Laboratories, Inc. (Andover, MA). Petroleum ether (hexanes, 55% *n*-hexane) was purchased from Fisher and dried and distilled over sodium and benzophenone (Fisher) before use.

3.2. Polymer synthesis

The homopolymers, poly(SA) and poly(CPH), were synthesized as previously reported [4]. Briefly CPH diacid was synthesized by a method similar to that described by Conix [39] for 1,3-bis(*p*-carboxyphenoxy)propane and purified by recrystallization from *N*-methyl-2-pyrolidinone three times. CPH and SA diacids were acetylated to form the prepolymers by refluxing in excess acetic anhydride for 30 min (SA) or 60 min (CPH) under dry nitrogen sweep. Purification of the crude prepolymers was done using the methods previously reported [4].

Melt polycondensation of the prepolymers was performed at 180 °C under vacuum (<0.5 mm Hg) for 90 min. About 2 ml of acetic anhydride was added to 4 g of prepolymer prior to polymerization to ensure complete acetylation. The polymer was isolated by dissolution in methylene chloride and precipitation in dry hexane, followed by filtration and drying under vacuum. The polymers were desiccated under dry argon to prevent degradation. Blends were formed by co-dissolution in chloroform or methylene chloride, and evaporation at room temperature with gentle agitation when dry samples were required.

3.3. Polymer characterization

Polymers were characterized by ^{1}H NMR in deuterated chloroform on a Varian VXR 300 MHz spectrometer (Varian Inc. Palo Alto, CA). Molecular weight was assessed via gel permeation chromatography (GPC). GPC samples

were dissolved in HPLC-grade chloroform and separation was done using PL Gel columns from Polymer Laboratories (Amherst, MA) on a Waters GPC system (Milford, MA). 50 μl samples were eluted at 1 ml/min. Elution times were compared to poly(methyl methacrylate) standards from Fluka (Milwaukee, WI). Differential scanning calorimetry on a DSC-7 (Perkin–Elmer, Shelton, CT) was used to characterize the thermal transitions of the polymers. Samples were heated at 5 °C/min and the data were taken on the second heating cycle. The molecular properties are listed in Table 1. The polycondensation synthesis typically results in high polydispersity index as noted in Table 1.

3.4. SAXS experiments

Samples for SAXS were prepared by melting the polymer into custom aluminum sample holders with a thickness of 35 μm. These make ideal sample holders because the aluminum is fairly transparent to 12 keV X-rays used in these experiments, and the rigid pans maintain the sample thickness when the polymer is melted in the vertically mounted SAXS sample chamber. The sample thickness was 2.2 mm. SAXS measurements were carried out on the instrument at 12-ID beam line at the Advanced Photon Source [40]. A 15 cm × 15 cm CCD detector was used to measure the intensity of scattering and the direct beam intensity was measured using a photodiode. The sample chamber was equipped with a custom furnace for heating the samples without interfering with the beam, permitting in situ data collection. A 50:50 (v/v) blend sample was used and data were collected at 140, 150, 160 and 170 °C. We know from prior experiments that the blend would be phase separated at room temperature [14]. And, because we perform copolymerization under vacuum at 180 °C, yielding random copolymers [8], we anticipate that the blend would become miscible as the temperature approaches 180 °C.

Five data sets were collected at each temperature with exposure times of 0.5 s at an incident beam energy of 12 keV ($\lambda = 1.035$ Å). The distance between the detector and the sample was 4 m. The scattering data were appropriately corrected and azimuthally averaged to obtain $I'(q)$.

The one-dimensional data were averaged for the five runs to obtain a single one-dimensional data set for each condition. These data were then corrected by subtracting the scattering due to a blank aluminum holder and normalized to an absolute scale with a polyethylene standard according to

$$I(q) = I'(q) \times \frac{25.4\ \mathrm{cm}^{-1}}{I'_{\mathrm{PE}}(q = 0.0245)} \times \frac{d_{\mathrm{PE}}}{d_{\mathrm{sample}}} \tag{14}$$

Here $I(q)$ represents the normalized intensity on an absolute scale, $I'P_{\mathrm{E}}$ is the intensity of the polyethylene standard measured at identical configuration, and d_{PE} and d_{sample} are respectively, the thicknesses of the PE standard (0.078 cm) and the sample, measured with a micrometer. The PE standard produces a peak at $q = 0.0245$ Å^{-1} whose absolute intensity is 25.4 cm^{-1}.

Table 1
Molecular properties of polymers used in this study

Polymer	M_n	PDI	T_g (°C)	T_m(°C)
Poly(CPH)	14,000	2.5	47	143
Poly(SA)	10,000	3.5	60	82

3.5. AFM experiments

Silicon wafers (approximately 1.5 cm × 1.5 cm) were cleaned by a modified version of the RCA clean procedure [41]. Briefly, wafers were soaked for ten minutes in an organic clean solution (70:15:15 deionized water:ammonium hydroxide:hydrogen peroxide), rinsed, and then soaked for ten minutes in an ionic clean solution (70:15:15 deionized water:hydrochloric acid:hydrogen peroxide). Both solutions were at 70–80 °C. No etch solution was used. Wafers were then cleaned using a CO_2 Snow Jet (Applied Surface Technologies, New Providence, NJ). A 20 nm layer of gold was deposited on the wafers by sputter coating. Films were spun cast at 1500 rpm for 30 s using a spin coater (Headway Research Inc., Garland, TX) from a 1% (w/v) solution of polymer in HPLC-grade chloroform, filtered through 0.2 μm PVDF membrane syringe filters (Pall Gelman, Portsmouth, UK) onto the gold-coated silicon wafers. This procedure results in films of uniform thickness of 200 nm. Films were dried at room temperature and atmospheric pressure for one hour. Films were annealed at temperatures of interest for up to 12 h under vacuum ($< 10^{-4}$ Torr) in a custom built annealing oven equipped with a hot stage, turbo molecular pump, roughing pump, and vacuum gauge (MKS Instruments, Boulder, CO). Annealed films were quenched on dry ice under dry argon to below the glass transition temperature, in order to 'freeze' the phase morphology prior to AFM experiments.

AFM images were obtained on a Dimension 3000 Scanning Probe Microscope (Digital Instruments, Santa Barbara, CA). The AFM was operated in contact mode using an Ultrasharp silicon cantilever (Mikromasch, Tallinn, Estonia) with a force constant of 0.30 N/m. All the films were about 200 nm thick, as measured by scratching the surface of the film and performing a line profile measurement with the AFM. Root-mean-square roughnesses were computed from AFM measurements as well.

3.6. Optical microscopy

Round glass coverslips from Fryer Company Inc. (Bloomington, MN) were cleaned by treatment in acetone,

methanol, and chloroform at room temperature. Samples for optical microscopy were spun cast (500 rpm, 30 s) onto the coverslips from 10% (w/v) solutions of polymer blends in HPLC-grade chloroform filtered with 0.2 μm PVDF membrane syringe filters. The resulting films were approximately 50–100 μm thick. Samples were dried in air and observed under a Nikon Eclipse ME600L microscope (Fryer) in reflected light mode using a 100 × long-working-distance objective. The microscope was equipped with a CCD camera (Hitachi Kokusai Electric Inc., Tokyo, Japan) and an A-200 heating stage (Fryer). The long working distance objective is necessary to protect the optics from the heating stage.

3.7. Molecular dynamics simulations

The MD simulations were conducted on a Dell Optiplex™ PC with an Intel® Pentium® 4 (3.06 GHz) processor and 1024 GB of RAM. The model systems were constructed using the Amorphous Cell module of the Materials Studio® 2.1 software package (Accelrys Inc., San Diego, CA).

4. Results and discussion

4.1. Phase diagram from SAXS

The SAXS data for the melts had significant contribution from voids especially in the low q region. The fast decay of the scattering from the voids becomes insignificant at $q > 0.01$ Å^{-1}. This parasitic scattering from the voids, I_p, behaves as

$$I_p \sim \frac{C}{q^4} \tag{15}$$

and must be subtracted. Provided that the voids have radii larger than the radii of gyration of the polymer chains, the constant, C, can be determined from the intercept of a plot of Iq^4 vs. q^4 [42]. The region over which this correction is fit was chosen as the region below the Debye region from the Kratky–Porod plot [30]. The corrected scattering data are shown in Fig. 2, and the Zimm plots of the same data at four temperatures are shown in Fig. 3. Interaction parameters were obtained from the intercepts of the Zimm plots following Eq. (11). The values of the interaction parameter are plotted in Fig. 4, from which the temperature dependence of χ can be extracted as:

$$\chi = -2.04 + \frac{802}{T} \tag{16}$$

Because χ decreases with temperature, the system becomes less miscible at lower temperatures, and an upper critical solution temperature (UCST) is predicted. This is consistent with the observations noted earlier. The critical temperature ($\chi = \chi_s$) for the particular molecular weights studied here is

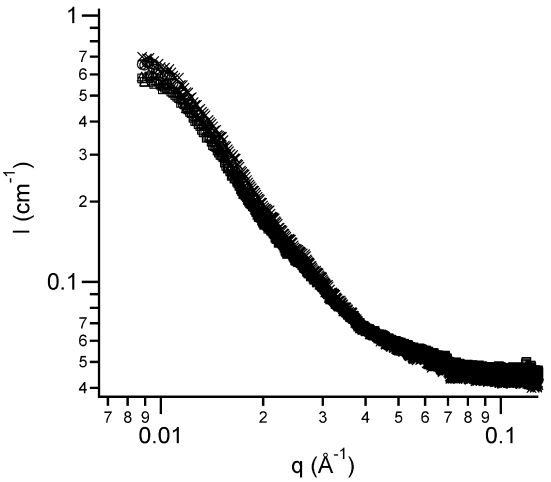

Fig. 2. Corrected SAXS data for poly(CPH)/poly(SA) blend at $T = 140$ °C (×), 150 °C (○), 160 °C (△), and 170 °C (□).

114 °C (from Eqs. (10) and (16)). The mean square radius of gyration, R_ϕ^2, is determined from the slope in the Zimm plot by Eq. (11). The average value of R_ϕ is 107 Å. The relatively high value of the R_ϕ results from the high polydispersity of these polymers (see Table 1) as the R_ϕ from scattering corresponds to the z-average radii of gyration of the polymers [43].

Eq. (16) can now be used in conjunction with the Flory–Huggins formulation of ΔG_{mix} (Eq. (1)) to predict the phase diagram. The spinodal curve (boundary between metastable and unstable regions) is defined by the locus of inflections in $\Delta G_{mix}/RT$ vs. ϕ plotted on the $T-\phi$ plane [31]. And, the binodal curve (boundary between metastable and stable regions) is the locus of points of common tangency (equal chemical potential) in $\Delta G_{mix}/RT$ vs. ϕ plotted on the $T-\phi$ plane [31]. The phase diagram obtained is shown in Fig. 5.

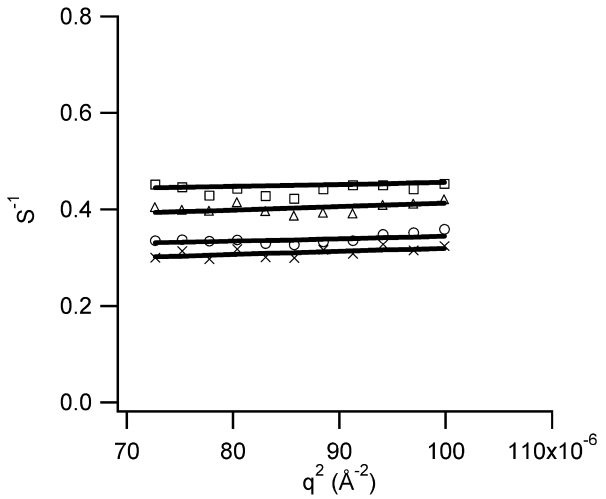

Fig. 3. Zimm plot of corrected SAXS data for $T = 140$ °C (×), 150 °C (○), 160 °C (△), and 170 °C (□).

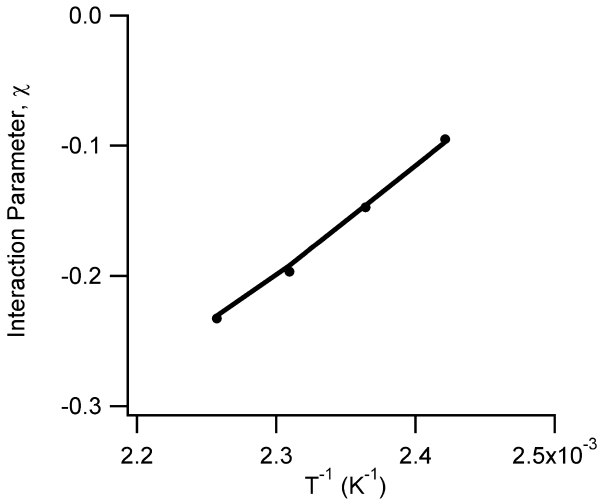

Fig. 4. Temperature dependence of χ obtained from SAXS.

4.2. Cloud point curve from optical microscopy

In order to verify the phase diagram obtained from the SAXS experiments, we performed in situ optical microscopy of blend films on a heating stage and recorded the cloud points. Below the critical point of the blend, phase separation is apparent, as concentration fluctuations in the film make the film appear cloudy. Upon heating through the first-order phase transition, the film homogenizes and becomes transparent. The cloud points for the poly (CPH)/poly(SA) blend system are plotted in Fig. 5 along with a prediction of the binodal and spinodal curves predicted for the blends used to make the microscopy samples.

The cloud point curve closely matches the predicted binodal curve. The error bars on the cloud point data indicate the 5 °C confidence with which the temperature of the film is controlled and the cloud points can be accurately observed.

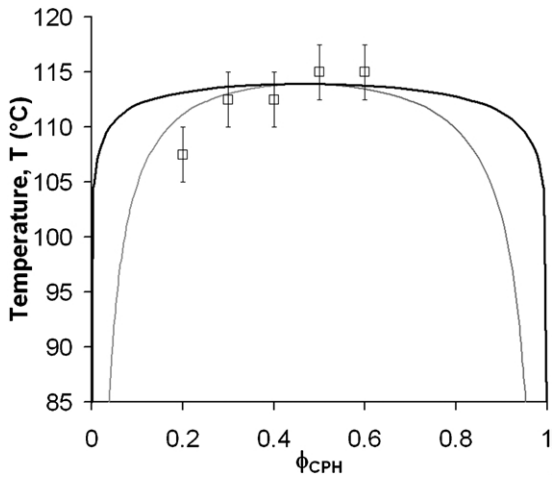

Fig. 5. Phase diagram for poly(CPH)/poly(SA) blend system obtained from SAXS, and cloud point data from optical microscopy (□). The spinodal curve is indicated by the gray line, and the binodal curve is indicated by the black line.

Cloud points can only be obtained in regions of the phase diagram where inhomogeneities due to crystallinity are not observed. (Both poly(SA) and poly(CPH) are semicrystalline, as stated before.) For compositions rich in poly(SA) crystallinity does not interfere, as poly(SA) melts at 82 °C. Unfortunately, poly(CPH) has a melting point above the critical point of the blend and a glass transition temperature of only 47 °C. (See Table 1.) So attempts to anneal blend films to rid them of poly(CPH) crystals are thwarted by crystallization during the cloud point observation. A further complication is that the length scale of the phase separation is very near the limits of the resolution of the microscope, so inhomogeneities due to amorphous phase separation cannot be discerned from those due to crystallinity. As the poly(CPH) content was increased, the apparent cloud point approached the melting temperature of poly(CPH) (143 °C), indicating that what was observed was actually the transition in the crystalline phase. Therefore, we were unable to accurately discern the cloud point for blend samples rich in poly(CPH) from in situ optical microscopy.

4.3. AFM for validating the CPH-rich region of the phase diagram

Observation of cloud points in the poly(CPH)-rich region of the phase diagram requires microscopic methods with higher resolution than that provided by optical microscopy, so that crystallinity can be discerned from amorphous phase separation. To accomplish this, ex situ atomic force microscopy (AFM) experiments were performed. It was not our goal with the AFM experiments to actually find the cloud point, as this would be very inefficient without the ability to perform AFM in situ. Rather we performed the AFM experiments in order to: A) determine an approximate length scale for the phase separation to verify that the cloud points observed in optical microscopy are real; and B) determine whether the predicted phase diagram accurately described the phase behavior in the poly(CPH)-rich region. Table 2 shows the compositions and temperatures studied. A temperature of 180 °C was chosen because this is the temperature at which we perform melt polycondensation to make copolymers. The 47:53 and 78:22 compositions were chosen because these are compositions from which we make copolymers.

Table 2
RMS roughness of blend films obtained from AFM experiments

Blend composition	RMS roughness (nm)		
	Room temperature	90 °C	180 °C
47:53 CPH:SA	39.2[a]	32.8[a]	7.7
78:22 CPH:SA	73.5[a]	54.1[a]	4.2

[a] Indicates phase-separated systems.

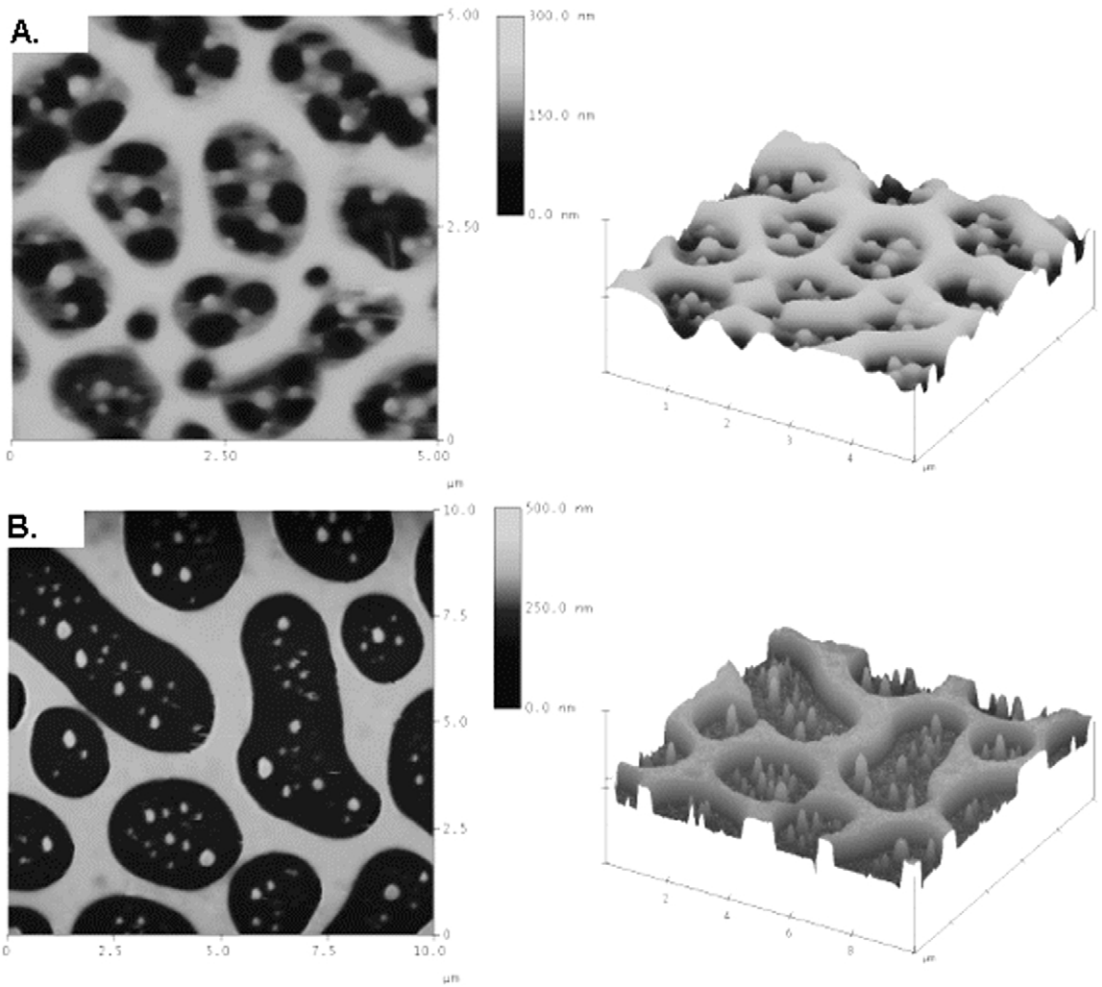

Fig. 6. AFM scans of as-cast poly(CPH)/poly(SA) blend films. (A) 5 μm × 5 μm scan of 47:53; (B) 10 μm × 10 μm scan of 78:22. RMS roughness is shown in Table 2.

The AFM scans obtained are shown in Figs. 6–8. We observe that for thin films, the length scale of the phase separation is on the order of 1 μm (Figs. 6(A) and (B), and 7), which is about the limit of resolution of the optical microscope. Fig. 6 shows clear evidence of phase separation in the 47:53 and 78:22 blends at room temperature. The phase separation persists in the films annealed at 90 °C (Fig. 7). Fig. 8 shows the 47:53 and 78:22 blend films annealed at 180 °C. The root-mean-square roughnesses obtained from AFM are summarized in Table 2. It is instructive to note that the surface roughnesses for the phase-separated films are an order of magnitude higher than those for the homogenous films. The phase behavior observed in the AFM scans is consistent with the phase diagram shown in Fig. 5.

4.4. MD simulations to predict energetic and structural parameters

We conducted molecular dynamics simulations using the Amorphous Cell® algorithm described earlier to predict E_{coh} for each of the homopolymers and the 51:49 poly(CPH)/poly(SA) blend. Systems were constructed in cubic simulation boxes with periodic boundary conditions, using a modification of Flory's rotational isomeric states (RIS) theory, employing the Meirovich scanning method [44]. This method looks ahead six bonds, while considering a maximum of 128 configurations when constructing the amorphous cells. The boxes were constructed according to the parameters in Table 3, containing CPH tetramers (80 backbone bonds) and/or SA heptamers (81 backbone bonds). The acid end groups of each chain were acetylated to eliminate the otherwise unrealistic concentration of acidic protons. For each set of conditions, five simulation boxes were constructed at a density of 0.6 g/cm^3. The raw structures were equilibrated to the target density via subsequent NPT molecular dynamics. Special care was taken to ensure that speared and catenated phenyl rings were eliminated. Where necessary, configurations were manually repaired followed by short NVT molecular mechanics runs (1000 steps) to equilibrate the structures.

Experimental densities for polyanhydrides are not

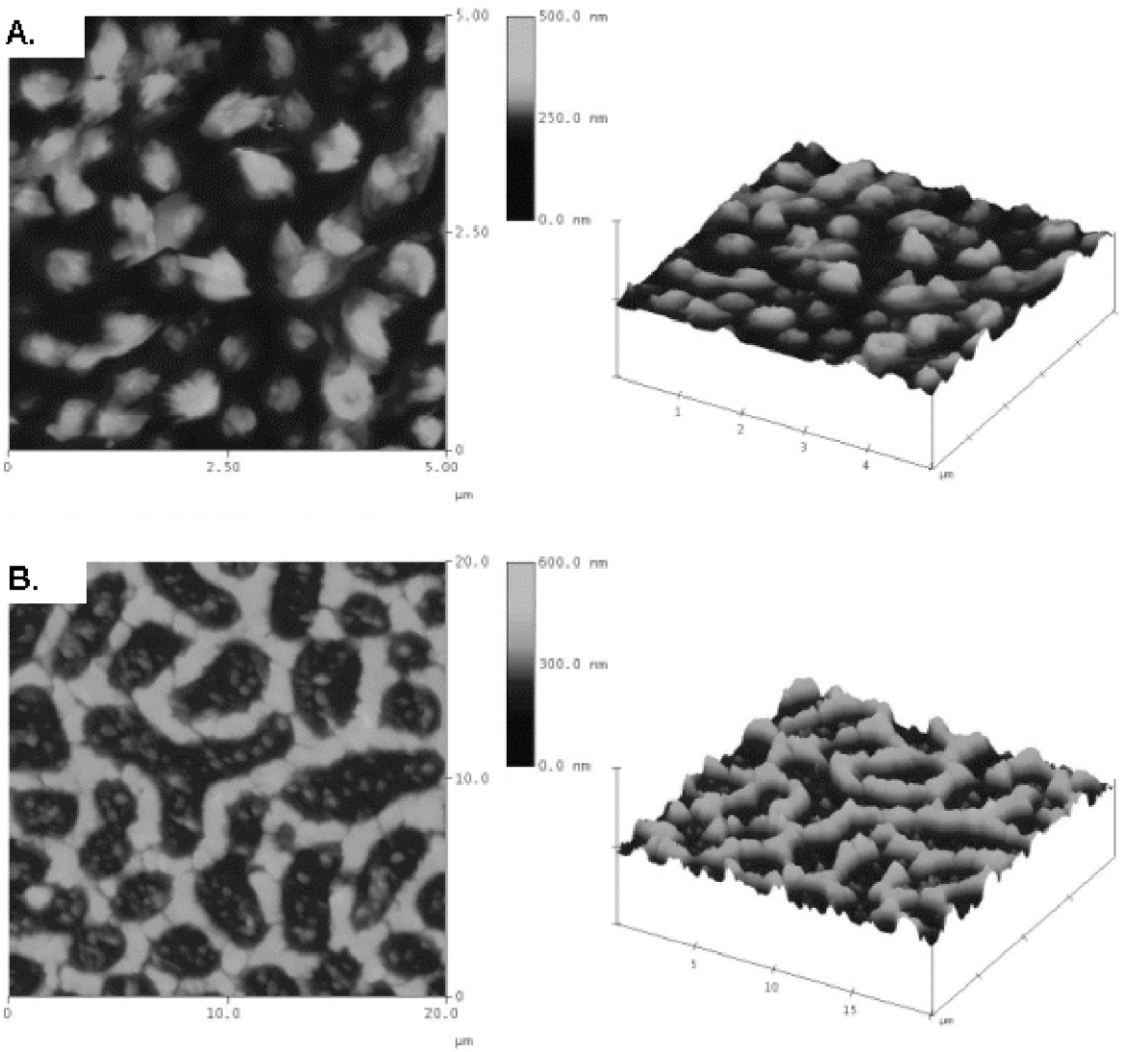

Fig. 7. AFM scans of poly(CPH)/poly(SA) blend films after annealing at 90 °C and $< 10^{-4}$ Torr. (A) 5 μm × 5 μm scan of 47:53; and (B) 20 μm × 20 μm scan of 78:22. RMS roughness is shown in Table 2.

reported in the literature, though Thomas et al. [3] estimate a density of 1.1 g/cm^3. We predicted the densities listed in Table 3 via NPT molecular dynamics simulations using the Andersen thermostat and Andersen barostat [45]. Van der Waals and Coulombic interactions were both summed by the Ewald method. (See description in [46] and references therein.) Runs of 100 ps (100,000 time steps of 1 fs) were required to equilibrate the density.

NVT MD simulations were then used to predict cohesive energy densities using the Andersen thermostat [45]. Simulations were run for 400 ps (400,000 time steps of 1 fs). The cell multipole method [47] was used for computing Coulombic interactions. At each temperature, the cohesive energy densities were sampled at 4 ps intervals. Temperature and potential energy were monitored at 1-ps intervals. The cohesive energy density was averaged over

Table 3
Parameters used to define simulation boxes for NVT MD simulations

Composition	# of atoms	Temperature (K)	Density (g/cm^3)	Box length (nm)
Poly(CPH) (8 CPH tetramers)	1544	363	1.1192	25.90
		453	1.0756	26.24
51:49 Blend (4 CPH tetramers, 4 SA heptamers)	1636	363	1.0656	26.11
		453	1.0185	26.50
Poly(SA) (8 SA heptamers)	1728	363	1.0017	25.20
		453	0.9397	26.99

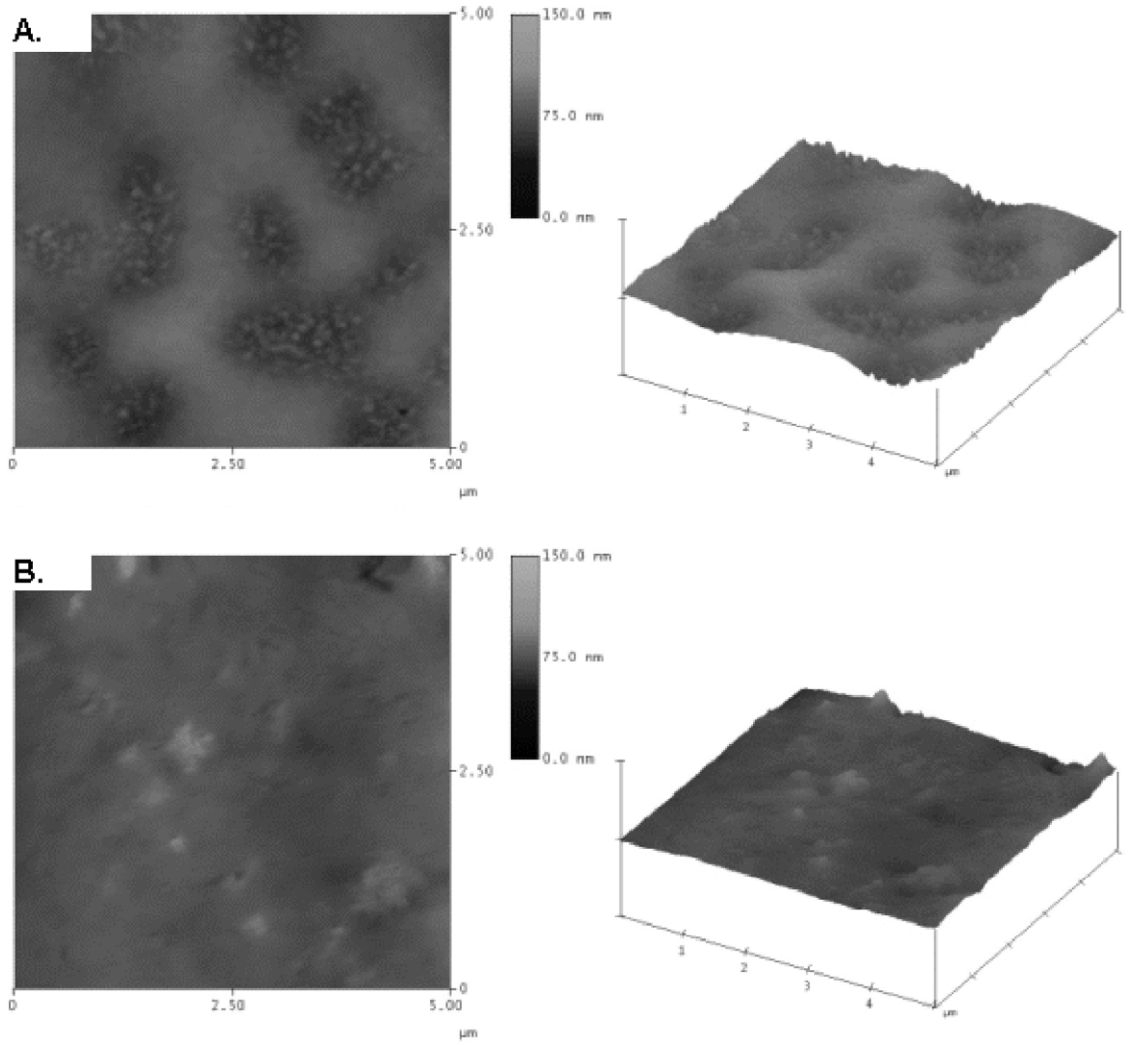

Fig. 8. AFM scans of poly(CPH)/poly(SA) blend films after annealing at 180 °C and $< 10^{-4}$ Torr. (A) 5 μm × 5 μm scan of 47:53 and (B) 5 μm × 5 μm scan of 78:22. RMS roughness is shown in Table 2.

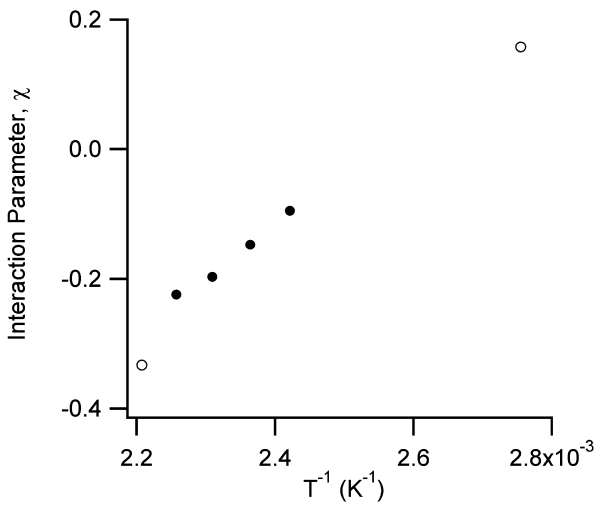

Fig. 9. Comparison of χ values obtained from SAXS (●) and those computed from molecular dynamics (○).

each of several starting configurations for each set of conditions. The energies of mixing were computed according to Eq. (12) and the interaction parameter was computed according to Eq. (13). The values for χ are plotted in Fig. 9 along with the values obtained from SAXS. These results are consistent, validating extrapolation of SAXS χ into the miscible region of the phase diagram, and demonstrating the value of the MD approach to predict energetics of the poly(CPH)/poly(SA) blend system.

The molecular simulations permit the calculation of a variety of interesting structural parameters. In particular, characteristic ratios can be estimated ($C_{\infty,\mathrm{CPH}} = 6.8$ and $C_{\infty,\mathrm{SA}} = 4.8$). These parameters will be used in future mesoscale studies, along with the predicted interaction parameters to investigate the phase behavior of both random and block copolymers.

We compare the results from the molecular simulations to solubility parameter predictions based on a group contribution method. The method of Fedors (reproduced

Table 4
Solubility parameter predictions from the group contribution method of Fedors reproduced in [27]. Solubility parameters are reported at 298 K

Compound	E_{coh}/V (J/cm^3)	δ (J/cm^3)$^{1/2}$
Poly(CPH)	443.6	21.1
Poly(SA)	390.1	19.8
Chloroform[a]		19.0
Methylene chloride[a]		19.8

[a] Data from [26].

in [27]) was used to compute E_{coh}, which was scaled with our predictions of the densities to get E_{coh}/V. The results are reported in Table 4 and compared to the solubility parameters of known solvents. The interaction parameter for the poly(CPH)/poly(SA) blend computed from Eq. (5) is 0.125 at 298 K. However, from Eq. (16), the value of χ is 0.65. The solubility parameters obtained from the group contribution method have no temperature dependence, so the critical temperature can be computed by rearranging Eq. (5) and computing the spinodal interaction parameter from Eq. (10). The critical temperature obtained in this way from the solubility parameters is 812 °C. Clearly, the solubility parameter approach is insufficient for accurately predicting the phase behavior of this system.

5. Conclusions

The phase behavior of the poly(CPH)/poly(SA) blend system was studied by measuring the CPH-SA segmental interaction parameter, χ, using in situ SAXS experiments. The predicted phase diagram is in good agreement with the cloud point measurement of poly(SA)-rich blends using optical microscopy. However, it was impossible to obtain cloud points for poly(CPH)-rich blends by optical microscopy, due to crystallinity, so this region of the predicted phase diagram was validated by AFM. The information from these three complementary techniques provides a complete description of the phase diagram of this system. The use of molecular dynamics to study this system was validated by the prediction of the cohesive energy density and comparison to the experimental results. Both the experimental methods and the computational techniques were shown to be superior to the solubility parameter approach.

More importantly, the accurate temperature dependence of χ can now be used to predict the phase behavior of copolymer systems that is of interest for drug delivery applications. Knowledge of the phase behavior will enable the development of accurate drug release models and the rational design of controlled release devices.

Acknowledgements

We wish to thank the Whitaker Foundation for financial support. We are grateful to Luke Brubaker, an undergraduate research assistant in the Chemical Engineering Department at Iowa State University for help with the polymer synthesis and characterization, and Dr Hajime Takano for his expertise on AFM. This work benefited from the use of BESSRC-CAT at APS and IPNS, funded by the U.S. DOE, BES under contract W-31-109-ENG-38 to the University of Chicago.

References

[1] Tamada J, Langer R. Biomater Sci Polym Ed 1992;3:315–53.
[2] Chiba M, Hanes J, Langer R. Biomaterials 1997;18:893–901.
[3] Thomas PA, Padmaja T, Kulkarni MG. J Controlled Release 1997;43:273–81.
[4] Kipper MJ, Shen E, Determan A, Narasimhan B. Biomaterials 2002;23:4405–12.
[5] Castellanos IJ, Cuadrado WL, Griebenow K. J Pharm Pharmacol 2001;53:1099–107.
[6] Truong VL, Williams JR, Hildreth JEK, Leong KW. Drug Delivery 1995;2:166–74.
[7] Mathiowitz E, Langer R. J Controlled Release 1987;5:13–22.
[8] Shen E, Kipper MJ, Dziadul B, Lim M-K, Narasimhan B. J Controlled Release 2002;82:115–25.
[9] Tabata Y, Gutta S, Langer R. Pharm Res 1993;10:487–96.
[10] Ron E, Turek T, Mathiowitz E, Chasin M, Hageman M, Langer R. Proc Nat Acad Sci USA 1993;90:4176–80.
[11] Katti DS, Lakshmi S, Langer R, Laurencin CT. Adv Drug Delivery Rev 2002;54:933–61.
[12] Narasimhan B, Kipper MJ. Adv Chem Engng 2004;29:169–218.
[13] Shen E, Pizsczek R, Dziadul B, Narasimhan B. Biomaterials 2001;22:201–10.
[14] Shen EE, Chen H-L, Narasimhan B. Proc Mat Res Soc 2001;662:NN421–5.
[15] Berkland C, Kipper MJ, Kim KK, Narasimhan B, Pack DW. J Controlled Release 2004;94:129–41.
[16] Chasin M, Lewis D, Langer R. Biopharm Manuf 1988;1:33–9.
[17] Larobina D, Kipper MJ, Mensitieri G, Narasimhan B. AIChE J 2002;48:2960–70.
[18] Domb A. J Polym Sci A 1993;31:1973–81.
[19] Shakesheff KM, Chen X, Davies MC, Domb A, Roberts CJ, Tendler SJB, Williams PM. Langmuir 1995;11:3921–7.
[20] Chen X, McGurk SL, Davies MC, Roberts CJ, Shakesheff KM, Tendler SJB, Williams JR, Davies J, Dawkes AC, Domb A. Macromolecules 1998;31:2278–83.
[21] Chan C-K, Chu I-M. Biomaterials 2002;23:2353–8.
[22] Flory PJ. Principles of polymer chemistry. Ithaca, NY: Cornell University Press; 1953.
[23] Case FH, Honeycutt JD. Trends Polym Sci 1994;2:259–66.
[24] Fan CF, Olafson BD, Blanko M, Hsu SL. Macromolecules 1992;25:3667–76.
[25] Kipper MJ, Narasimhan B. In: Erickson LE, editor. Proceedings of the 31st Annual Biochemical Engneering Symposium. 2001. p. 65–72.
[26] Hildebrand JH, Scott RL. The solubility of nonelectrolytes. New York: Reinhold; 1950.
[27] Van Krevelen DW. Properties of polymers: their correlation with chemical structure; their numerical estimation and prediction from additive group contributions. New York: Elsevier; 1990.
[28] Tiller AR, Gorella B. Polymer 1994;35:3251–9.
[29] de Gennes P-G. Scaling concepts in polymer physics. Ithaca, NY: Cornell University Press; 1979.
[30] Roe R-J. Methods of X-ray and neutron scattering in polymer science. New York: Oxford University Press; 2000.

[31] Strobl G. The physics of polymers. Berlin: Springer-Verlag; 1997.
[32] Meier H, Strobl GR. Macromolecules 1987;20:649–54.
[33] Patnaik SS, Pachter R. Polymer 2002;43:415–24.
[34] Patnaik SS, Pachter R. Polymer 1999;40:6507–19.
[35] Eichinger BE, Rigby D, Stein J. Polymer 2002;43:599–607.
[36] Theodorou DN, Suter UW. Macromolecules 1985;18:1467–78.
[37] Flory PJ. Statistical mechanics of chain molecules. New York: Wiley-Interscience; 1969.
[38] Sun H. J Phys Chem B 1998;102:7338–64.
[39] Conix A. Macromol Synth 1966;2:95–8.
[40] Seifert S, Winans RE, Tiede DM, Thiyagarajan P. J Appl Cryst 2000; 33:782–4.
[41] Kern W, Puotinen DA. RCA Rev 1970;186–206.
[42] Koch T, Strobl GR. J Polym Sci B: Polym Phys 1990;28:343–53.
[43] Higgins JS, Benoît HC. Polymers and neutron scattering. Oxford: Clarendon Press; 1994.
[44] Meirovitch H. J Chem Phys 1983;79:502–8.
[45] Andersen HC. J Chem Phys 1980;72:2384–93.
[46] Frenkel D, Smit B. Understanding molecular simulation from algorithms to applications. San Diego: Academic Press; 2002.
[47] Ding H-Q, Karasawa N, Goddard WAI. J Chem Phys 1992;97: 4309–14.